Modeling the timing of Patagonian Ice Sheet retreat in the Chilean Lake District from 22-10 ka

Joshua Cuzzone[1], Matias Romero[2], Shaun A. Marcott[2]

[1]Joint Institute for Regional Earth System Science and Engineering, University of California, Los Angeles
[2]Department of Geoscience, University of Wisconsin, Madison

Correspondence to: Joshua K. Cuzzone (Joshua.K.Cuzzone@jpl.nasa.gov)

Abstract

Studying the retreat of the Patagonian Ice Sheet (PIS) during the last deglaciation represents an important opportunity to understand how ice sheets outside the polar regions have responded to deglacial changes in temperature and large-scale atmospheric circulation. At the northernmost extension of the PIS during the last glacial maximum (LGM), the Chilean Lake District (CLD) was influenced by the southern westerly winds (SWW), which strongly modulated the hydrologic and heat budget of the region. Despite progress in constraining the nature and timing of deglacial ice retreat across this area, considerable uncertainty in the glacial history still exists due to a lack of geologic constraints on past ice margin change. Where the glacial chronology is lacking, ice sheet models can provide important insight into our understanding of the characteristics and drivers of deglacial ice retreat. Here we apply the Ice Sheet and Sea-level System Model (ISSM) to simulate the LGM and last deglacial ice history of the PIS across the CLD at high spatial resolution (450 meters). We present a transient simulation of ice margin change across the last deglaciation using climate inputs from the CCSM3 Trace-21ka experiment. At the LGM, the simulated ice extent across the CLD agrees well with the most comprehensive reconstruction of PIS ice history (PATICE). Coincident with deglacial warming, ice retreat ensues after 19ka, with largescale ice retreat occurring across the CLD between 18 and 16.5 ka. By 17 ka the northern portion of the CLD becomes ice free, and by 15 ka, ice only persists at high elevations as mountain glaciers and small ice caps. Our simulated ice history agrees well with PATICE for early deglacial ice retreat but diverges at and after 15 ka, where the geologic reconstruction suggests persistence of an ice cap across the southern CLD until 10 ka. However, given the high uncertainty in the geologic reconstruction of the PIS across the CLD during the later deglaciation, this work emphasizes a need for improved geologic constraints on past ice margin change. While deglacial warming drove the ice retreat across this region, sensitivity tests reveal that modest variations in wintertime precipitation (~10%) can modulate the pacing of ice retreat by up to 2 ka, which has implications when comparing simulated outputs of ice margin change to geologic reconstructions. While we find that TraCE-21ka simulates large-scale changes in the SWW across the CLD that are consistent with regional paleoclimate reconstructions, the magnitude of the simulated precipitation changes is smaller than what is found in proxy records. From our sensitivity analysis we can deduce that larger anomalies in precipitation as found in paleoclimate proxies may have had a large impact on modulating deglacial ice retreat, highlighting an additional need to better constrain the deglacial change in the strength, position, and extent of the SWW as it relates to understanding the drivers of deglacial PIS behavior.

1 Introduction

During the Last glacial maximum (LGM), the Patagonian Ice Sheet (PIS) covered the Andes mountains from 38°S to 55°S, with an estimated sea-level equivalent ice volume of 1.5 meters (Davies et al., 2020). At the northernmost extent of the PIS, across an area presently known as the Chilean Lake District (CLD), the LGM to deglacial ice behavior and related climate forcings has been a subject of historical interest (Mercer, 1972; Porter, 1981; Lowell et al., 1995; Andersen et al., 1999; Denton et al., 1999; Glasser et al., 2008, Moreno et al., 2015; Kilian and Lamy, 2012; Lamy et al., 2010), and have served as important constraints towards understanding the drivers of ice sheet change across centennial to millennial timescales. Currently, PATICE (Davies et al., 2020) serves as the latest and most complete reconstruction of the entire PIS during the LGM and last deglaciation. Across the CLD (Figure 1), the LGM ice limits are well constrained by terminal moraines in the southwest and western margins (Denton et al., 1999; Glasser et al., 2008, Moreno et al., 2015). However, due to a lack of geomorphological and geochronologic constraints on past ice margin change, the reconstructed deglaciation remains highly uncertain.

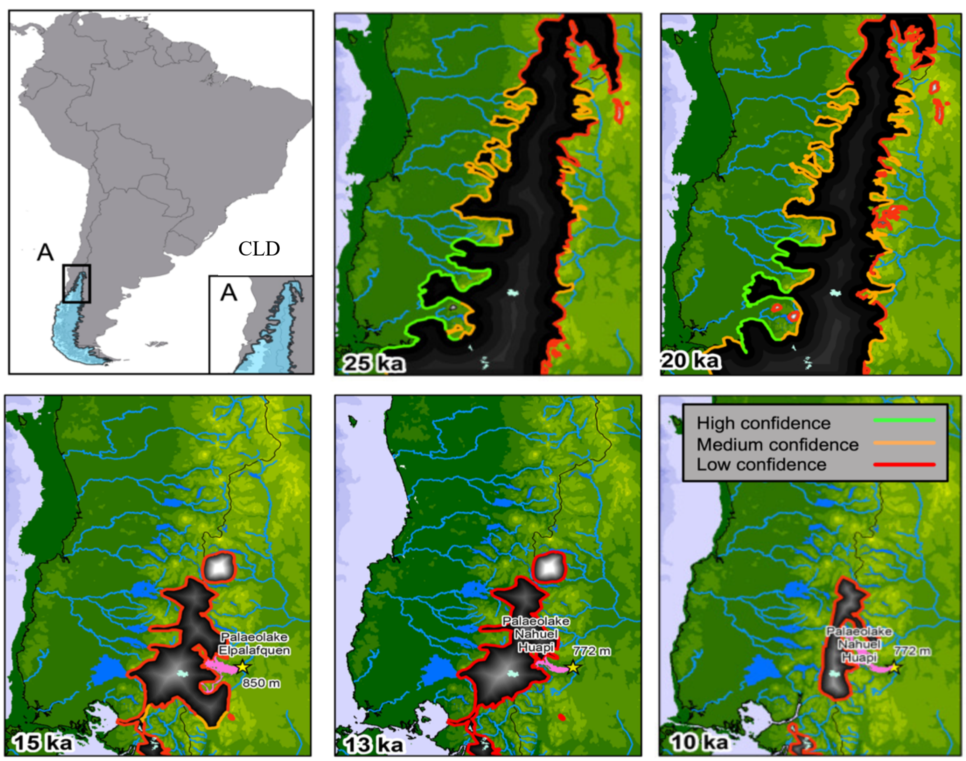

Figure 1. Location of the study area across the Chilean Lake District (CLD; Upper Left Panel). The reconstructed ice extent from PATICE for the PIS across the CLD at 25 ka, 20 ka, 15 ka, 13 ka, and 10 ka are taken from Davies et al., 2020. The color of the line marking the reconstructed ice extent corresponds to the confidence in the reconstruction as described in section 3.3.

While deglacial warming is a primary driver of ice retreat across the CLD, evidence suggests that variations in precipitation patterns influenced the timing and magnitude of this retreat (Moreno et al., 1999; Rojas et al., 2009). The wintertime climate across South America is strongly influenced by the southern westerly winds (SWW), which exert a large control on the synoptic scale hydrologic and heat budget (Garreaud et al., 2013). During the LGM and last deglaciation, paleoclimate data indicates that the position, strength, and extent of the SWW varied latitudinally, migrating southward during warmer intervals and northward during cooler intervals, ultimately altering overall ice sheet mass balance (Mercer, 1972; Denton et al., 1999; Lamy et al., 2010; Kilian and Lamy, 2012; Boex et al., 2013). Terrestrial paleoclimate proxies that indicate that the CLD was wetter during the LGM and early deglaciation have been used to support the idea that the SWW migrated northward of 41°S across the CLD (Moreno et al., 1999; Moreno et al., 2015; Moreno and Videla, 2018; Diaz et al., 2023). Additionally, these proxies indicate a switch from hyper humid to humid conditions around 17,300 cal yr BP, which was inferred by Moreno et al. (2015) to indicate the poleward migration of the SWW south of the CLD.

However, inferring changes in the SWW across the last deglaciation from paleoclimate proxies can be problematic as outlined by Kohfeld et al. (2013) who compiled an extensive dataset of paleoclimate archives that record changes in moisture, precipitation-evaporation balance, ice accumulation, runoff and precipitation, dust deposition, and marine indicators of sea surface temperature, ocean fronts, and biologic productivity. Kohfeld et al. (2013) conclude that environmental changes inferred from existing paleoclimate data could be potentially explained by a range of plausible scenarios for the state and change of the SWW during the LGM and last deglaciation, such as a strengthening, poleward or equatorward migration, or no change. Climate model results from Sime et al. (2013) indicate that the reconstructed changes in moisture from Kohfeld et al. (2013) can be simulated well without invoking large shifts or changes in strength to the SWW. This discrepancy also exists amongst climate models which diverge on whether the LGM SWW was shifted equatorward or poleward, and was stronger or weaker than present day (Togweiler et al., 2006; Menviel et al., 2008; Rojas et al., 2009; Rojas et al., 2013; Sime et al., 2013; Jiang et al., 2020). Therefore, from paleoclimate proxies and climate models, we still do not have a firm understanding of how the SWW may have changed during the last deglaciation, and how these variations may have influenced the deglaciation of the PIS.

Early paleo ice sheet modelling experiments across the PIS have focused on evaluating the relationship between the simulated LGM ice sheet geometry in response to spatially uniform temperature change (Hulton et al., 2002; Sugden et al., 2002; Hubbard et al., 2005). While these early simulations provided constraints on PIS areal extent, ice volume, and sensitivity to LGM temperature depressions, spatially varying temperature and precipitation were not considered. Recently, Yan et al. (2022) simulated the PIS behavior at the LGM using an ensemble of climate model output from the Paleoclimate Modelling Intercomparison Project (PMIP4; Kageyama et al., 2021). Results best matching the empirical reconstructions from PATICE (Davies et al., 2020) suggest that reduction in temperature was likely the main driver of PIS LGM extent, although the authors found that variation in regional LGM precipitation anomaly can have large impacts on the simulated ice sheet geometry. This evidence is supported by recent glacier modelling across the northeastern Patagonian Andes which suggests that increases in precipitation during the termination of the LGM are necessary to achieve modeled fit with reconstructed glacier extent (Muir et al., 2023; Leger et al., 2021). Additionally, Martin et al. (2022) found that precipitation greater than present day are needed to explain late glacial and Holocene ice readvance of the Monte San Lorenzo ice cap, lying to the southeast of the current Northern Patagonian Ice Field. These regional studies therefore provide further evidence that late glacial and deglacial variability in precipitation, perhaps driven by changes in the SWW, influenced PIS retreat and readvance over numerous timescales.

To advance our understanding of the last glacial and deglacial ice behavior across the CLD, we use a numerical ice sheet model to simulate the LGM ice geometry and deglacial ice retreat using transiently evolving boundary conditions from a climate model simulation of the last 21,000 years (TraCE-21ka; Liu et al., 2009; He et al., 2013) which simulates large scale variability in the strength and position of the SWW (Jiang and Yan, 2020). Because there is a lack of transiently evolving ice sheet model simulations of the PIS across the last deglaciation, our aim is to provide possible constraints on the nature of ice retreat across the CLD region, from which the reconstructions (PATICE; Davies et al., 2020) are uncertain. Also, by assessing the sensitivity of our ice sheet experiments to a range of climatic boundary conditions, we aim to provide additional insight into the dominant climatic controls on the deglacial evolution of the PIS in the CLD region.

2 Methods: Model description and setup

2.1 Ice sheet model

In order to simulate the ice margin migration across the CLD during the LGM and last deglaciation, we use the Ice Sheet and Sea-level System Model (ISSM), a thermomechanical finite-element ice sheet model (Larour et al., 2012). Because of the high topographic relief across the CLD and associated impact on ice flow, we use a higher-order approximation to solve the momentum balance equations (Dias dos Santos et al., 2022). This ice flow approximation is a depth-integrated formulation of the higher-order approximation of Blatter (1995) and Pattyn (2003), which allows for an improved representation of ice flow compared with more traditional approaches in paleo-ice flow modelling (e.g., Shallow Ice Approximation or hybrid approaches; Hubbard et al., 2005; Leger et al., 2022; Yan et al., 2022), while allowing for reasonable computational efficiency. Our model domain comprises the northernmost LGM extent of the PIS across the CLD, extending beyond the LGM ice extent reconstructed from Davies et al. (2020) and ends along the northern shore of the Golfo de Ancud (Figure 2).

We rely on anisotropic mesh adaptation to create a non-uniform model mesh that varies based upon gradients in bedrock topography from the General Bathymetric Chart of the Oceans (GEBCO; GEBCO Bathymetric Compilation Group, 2021), a terrain model for ocean and land. For the land component, the GEBCO model uses version 2.2 of the Surface Radar Topography Mission data (SRTM15_plus; Tozer et al., 2019), to create a 15 arc second gridded output of terrain elevation relative to sea level. Our ice sheet model horizontal mesh resolution varies from 3 km in areas of low bedrock relief to 450 meters in areas where gradients in the bedrock topography is high and comprises 40,000 model elements.

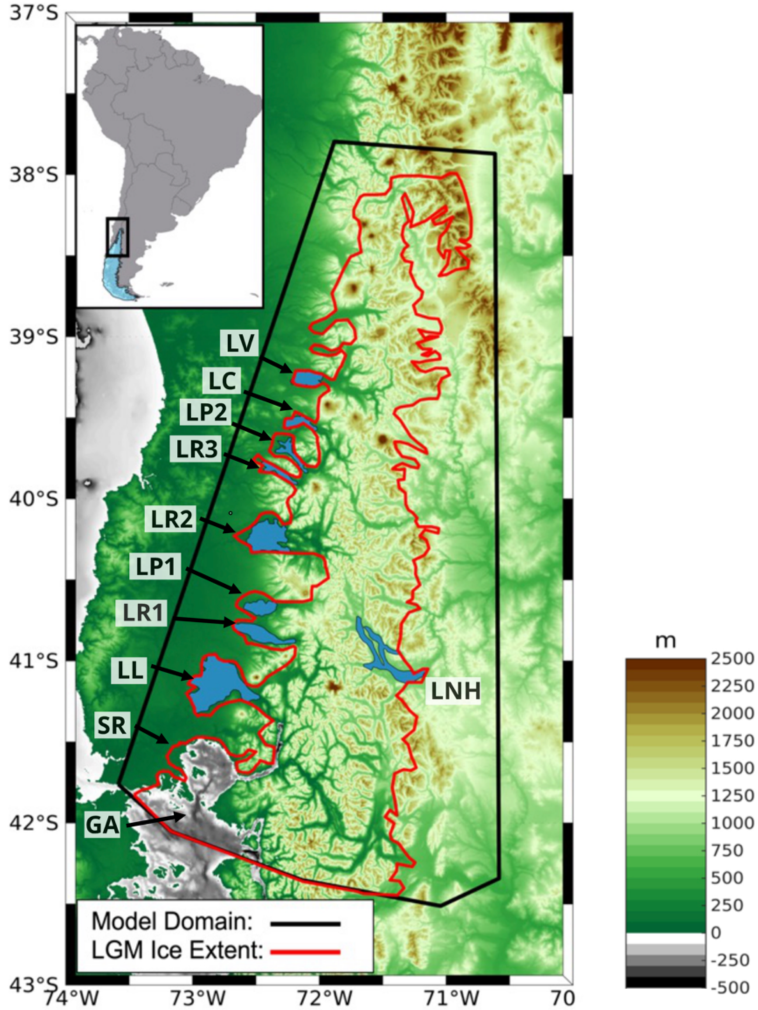

Figure 2. Bedrock topography for our study area (meters). Our model domain (shown as the black line), encompasses the reconstructed LGM ice limit (shown in red) from PATICE (Davies et al., 2020). Present day lakes are shown in blue, with abbreviated names as: SR (Seno de Reloncaví), GA (Golfo de Ancud), LL (Lago Llanquihue), LR1 (Lago Rupanco), LP1 (Lago Puyehue), LR2 (Lago Ranco), LR3 (Lago Riñihue), LP2 (Lago Panguipulli), LC (Lago Calafquén), LV (Lago Villarica), LNH (Lago Nahuel Huapi).

Although geomorphological evidence suggests that while southernmost glaciers across the PIS may have been temperate with warm based conditions during the LGM, there may have been periods where ice lobes were polythermal (Darvill et al., 2016). However, recent ice flow modelling (Leger et al., 2021) suggests that varying ice viscosity mainly impacts the accumulation zone thickness in simulations of paleoglaciers in Northeastern Patagonia, with minimal impacts on overall glacier length and extent. Accordingly, based on sensitivity tests (see supplement section S1), our model is 2-dimensional and we do not solve for ice temperature and viscosity allowing for increased computational efficiency. For our purposes, we use Glen's flow law (Glen, 1955) and set the ice viscosity following the rate factors in Cuffey and Paterson (2010) assuming an ice temperature of -0.2°C. We use a linear friction law (Budd et al., 1979)

$$\tau_b = -k^2 N v_b \tag{1}$$

where τ_b represents the basal stress, N represents the effective pressure, and v_b is the magnitude of the basal velocity. Here N = g(ρ_iH + ρ_wZ$_b$), where g is gravity, H is ice thickness, ρ_I is the density of ice, ρ_w is the density of water, and Z_b is bedrock elevation following Cuffey and Paterson (2010).

The spatially varying friction coefficient, k, is constructed following Åkesson et al. (2018):

$$k = 200 \times \frac{\min[\max(0, z_b + 600), z_b]}{\max(z_b)} \quad (2)$$

where z_b is the height of the bedrock with respect to sea level. Using this parameterization, basal friction is larger across high topographic relief and lower across valleys, and areas below sea level.

To account for the influence of glacial isostatic adjustment (GIA), we prescribe a transiently evolving reconstruction of relative sea level from the global GIA model of the last glacial cycle from Caron et al. (2018). This includes three physical components: 1) Bedrock vertical motion 2.) Eustatic sea level, and 3.) Geoid changes. The time series we use to prescribe GIA is from the model average of an ensemble of GIA forward model estimations from Caron et al., 2018. The prescribed GIA is in good agreement (Figure S2) with a reconstruction of relative sea-level change from an isolation basin in central Patagonia (Troch et al., 2022). This methodology has been applied in recent modelling following Cuzzone et al. (2019) and Briner et al. (2020).

2.2 Experimental Design

In order to simulate the ice history at the LGM and across the last deglaciation we use climate model output from the National Center for Atmospheric Research Community Climate System Model (CCSM3) TraCE-21ka transient climate simulation of the last deglaciation (Liu et al., 2009; He et al., 2013). Monthly mean output of temperature and precipitation are used from these simulations as inputs to our glaciological model (full climate forcings details are further described in section 2.4) and we use the monthly mean output every 50 years across the last deglaciation. Large, multi-proxy reconstructions from He and Clark (2022), Liu et al. (2009), He et al. (2011), and Shakun et al. (2012; 2015) have all demonstrated good agreement between TRACE 21k and a wide variety of paleo-proxy data during the last deglaciation that include records from the West Antarctic and South America.

2.3 Surface Mass Balance

In order to simulate the deglaciation of the PIS across our model domain we require inputs of temperature and precipitation to estimate the surface mass balance. To derive snow and ice melt we use a positive degree day model (Tarasov and Peltier, 1999; Le Morzadec et al., 2015; Cuzzone et al., 2019; Briner et al., 2020). Our degree day factor for snow melt is 3 mm ºC^{-1}day^{-1} and 6 mm ºC^{-1}day^{-1} for bare ice melt, and we use a lapse rate of 6 ºC/km to adjust the temperature of the climate forcings to surface elevation, which are within a range of typical values used to model contemporary and paleo glaciers across Patagonia (see Fernandez et al., 2016 Table 3; Yan et al., 2022). The hourly temperatures are assumed to have a normal distribution, of standard deviation 3.5 degrees Celsius around the monthly mean. An elevation-dependent desertification is included (Budd and Smith, 1981) which reduces precipitation by a factor of 2 for every kilometer change in ice sheet surface elevation. We note that the values in the surface mass balance parameters were chosen to provide a reasonable fit within 5% between the simulated LGM ice sheet area and the reconstructed ice area from PATICE (see Figure 10).

2.4 Climate forcings

In order to scale monthly temperature and precipitation across the LGM and last deglaciation we applied a commonly used modeling approach (Pollard et al., 2012; Seguinot et al., 2016; Golledge et al., 2017; Tigchlaar et al., 2019; Clark et al., 2020; Briner et al., 2020; Cuzzone et al., 2022; Yan et al., 2022; equations 3 and 4). First, we use the monthly mean climatology of temperature and precipitation for the period 1979-2018 ($\bar{T}_{(1979-2018)}, \bar{P}_{(1979-2018)}$) from the Center for Climate Resilience Research Meteorological dataset version 2.0 (CR2MET; Boisier et al., 2018). This output, which uses information from a climate reanalysis and is calibrated against rain-gauge observations, is provided at 5 km spatial resolution. We then bilinearly interpolate these fields onto our model mesh.

$$T_t = \bar{T}_{(1979-2018)} + \Delta T_t \tag{3}$$

$$P_t = \bar{P}_{(1979-2018)} + \Delta P_t \tag{4}$$

Next, anomalies of the monthly temperature and precipitation fields are computed as the difference from the preindustrial control run and interpolated onto our model mesh (ΔT_t and ΔP_t). These anomalies are added to the contemporary monthly mean as shown in equations 3 and 4, to produce the monthly temperature and precipitation fields at LGM and across the last deglaciation (T_t and P_t).

2.5 Ice front migration and iceberg calving

We simulate calving where the PIS interacts with ocean. We track the motion of the ice front using the level-set method described in Bondzio et al. (2016; equation 3) in which the ice velocity (v_f) is a function of the ice velocity vector at the ice front (v), the calving rate (c), the melting rate at the calving front ($\dot{M}$), and where n is the unit normal vector pointing horizontally outward from the calving front. For these simulations the melting rate is assumed to be negligible compared to the calving rate, so $\dot{M}$ is set to 0.

$$v_f = v - (c + \dot{M})\, n \tag{5}$$

To simulate calving we employ the more physically based Von Mises stress calving approach (Morlighem et al., 2016) which relates the calving rate (c) to the tensile stresses simulated within the ice, where $\tilde{\sigma}$ is the von Mises tensile strength, $\|v\|$ is the magnitude of the horizontal ice velocity, and σ_{max} is the maximum stress threshold which has separate values for grounded and floating ice.

$$c = \|v\| \frac{\tilde{\sigma}}{\sigma_{max}} \tag{6}$$

The ice front will retreat if von Mises tensile strength exceeds a user defined stress threshold, which we set to 200 kPa for floating ice and 1 MPa for tidewater ice. This calving law has been applied in Greenland to assess marine terminating icefront stability (Bondzio et al., 2016; Morlighem et al., 2016; Choi et al., 2021; Cuzzone et al., 2022) and for our simulations applies where ocean is present such as the Seno de Reloncaví and the Golfo de Ancud (see Figure 2).

3 Results

3.1 Simulated LGM state

In order to arrive at a steady state LGM ice geometry, we first initialize our model with an ice-free configuration. A constant LGM monthly climatology of temperature and precipitation are then applied, as well as the prescribed GIA from Caron et al. (2018). We allow the ice sheet to relax for 10,000 years, during which, the ice sheet is free to grow and expand until it reaches a steady state ice geometry and volume, in equilibrium with the climate forcings.

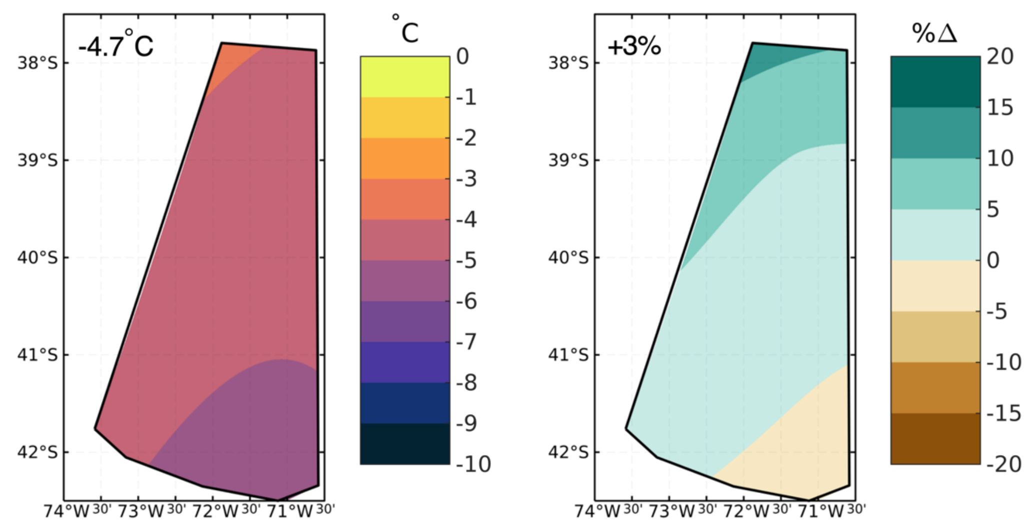

Figure 3. The LGM summer (DJF) temperature anomaly (left panel) and the LGM winter precipitation anomaly (right panel) from TraCE-21ka. Anomalies are taken as the difference between the LGM and preindustrial (LGM-PI), with the precipitation anomalies expressed as the percent difference of the LGM from preindustrial. The area averaged value of the anomaly is shown in the upper left of each panel.

At 22 ka, Trace-21ka simulates an area averaged summertime (DJF) cooling of 4.7°C relative to the PI across our model domain (Figure 3). The LGM cooling increases from north to south, with the greatest magnitude of cooling occurring across the southern portion of our model domain of up to 6°C. During winter (JJA), Trace-21ka simulates an overall wetter climate across our model domain during the LGM relative to the PI. While the area-averaged LGM precipitation anomaly is small (3% higher), the LGM precipitation anomaly increases from south to north, with Trace-21ka simulating 10-15% more wintertime precipitation during the LGM than the PI across the northern portion of the model domain. While the mean position of the wintertime SWW is simulated to be poleward during the LGM relative to the PI in TraCE-21ka (Jiang and Yan, 2022), the low-level zonal wind (925 hPa) is stronger during the LGM across our model domain and Patagonia (Figure S3A). We also find that relative to PI, wintertime low level (850 hPa) moisture flux convergence is higher during the LGM across our model domain (Figure S4A).

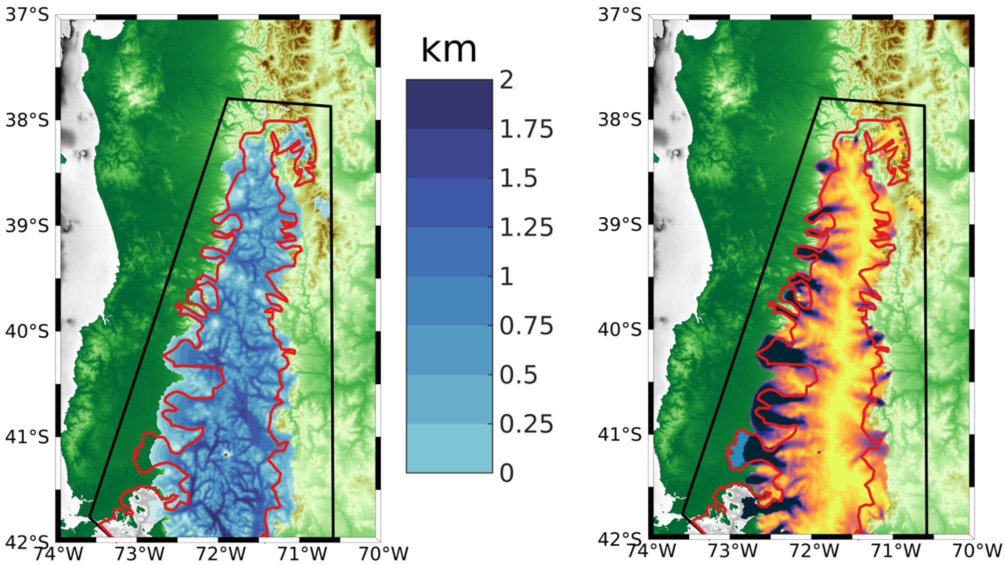

Figure 4. The simulated LGM ice thickness (km; left panel) and the simulated LGM ice surface velocity (km/yr; right panel) is shown. The black outline denotes our ice sheet model boundary, and the red line denotes the LGM reconstructed ice extent from PATICE (Davies et al., 2020).

Bedrock elevation increases from west to east, with deep valleys interspersed across most of our model domain (Figure 2). LGM ice thickness is greatest in these valleys (upwards of 2000 meters) where driving stresses dominate and where bedrock geometry controls the flow of ice from higher terrain and through these valleys. Across the highest terrain such as the many volcanoes across the CLD, ice is comparatively thinner than the surrounding valleys. An ice divide is present as slow ice velocities in the interior of the ice sheet, which give way to fast flowing outlet glaciers especially on the western margin of the CLD where velocities reach in excess of 500 m/yr and in some location up to 2 km/yr. The simulated LGM ice sheet area across the CLD is 414,120 km^2, which is within 1% of the area calculated from the PATICE reconstruction (414,690 km^2). This agreement is in part due to the tuning of our degree day factors as discussed in section 2.3, and gives confidence to our ability to simulate a reasonable LGM ice sheet across the CLD and throughout the last deglaciation.

3.2 Simulation of the Last Deglaciation

Monthly mean temperature and precipitation, taken every 50 years from the TraCE-21ka (Liu et al., 2009; He et al., 2013) experiment is used to drive our simulation of ice history across the last deglaciation (22 ka – 10 ka). The transient simulation is initialized with the LGM ice sheet geometry shown in Figure 4, and is run forward with the appropriate climate boundary conditions until 10 ka.

3.2.1 Pattern of Deglaciation

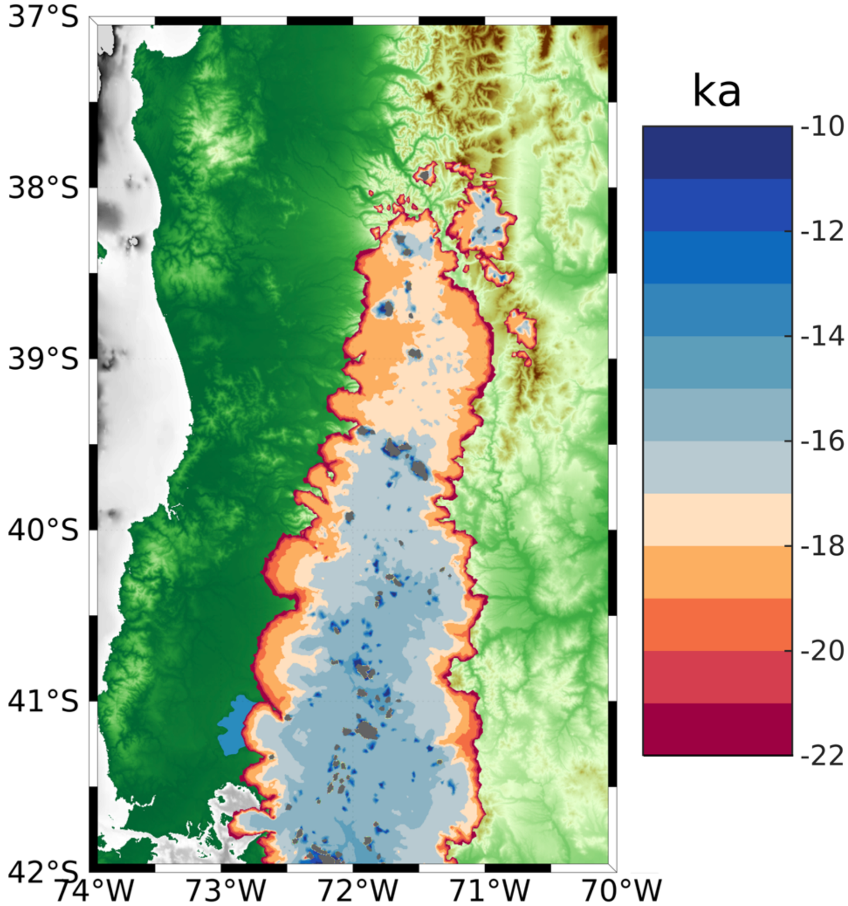

Figure 5. The simulated deglaciation age for the transient simulation from the LGM to 10 ka. The gray color indicates where ice persists after 10 ka.

From the resulting transient simulation, we calculate the timing of deglaciation across our model domain (Figure 5). Because of possible readvances during the deglaciation, we select the youngest age at which grid points become ice free. Our map of the simulated deglaciation can be paired with a timeseries of the rate of ice mass change (Figure 6) to highlight some key features in the magnitude and timing of ice retreat between 22 ka and 10 ka.

Between 22 ka to 19 ka, the ice sheet undergoes periods of minor to moderate ice mass loss and gain in an interval of time where summer temperature anomalies (Figure 6) and the corresponding ice margin remain relatively stable (Figure 5). Between 19 ka and 18.5 ka, coincident with a rise in summertime temperature (Figure 6), a pulse of ice mass loss exceeding 5,000 GT/century occurs before trending toward minimal ice mass loss around 18 ka as the rise in summer temperature levels off. During this time interval, the ice margin pulls back considerably towards higher terrain across the northern portion of the model domain (Figure 5), and many of the fast-flowing outlet glaciers on the western margin retreat back towards the ice sheet interior. Between 18 ka to 16.2 ka, summer temperature rises steadily ~1.2°C and is punctuated with an abrupt warming of ~0.5°C at 16 ka (Figure 6). During this interval, ice mass loss remains high and steady at ~1000

GT/century with pulses of increased mass loss at 17.8 ka, 16.8 ka, and 16 ka varying between 2000-5000 GT/century (Figure 6).

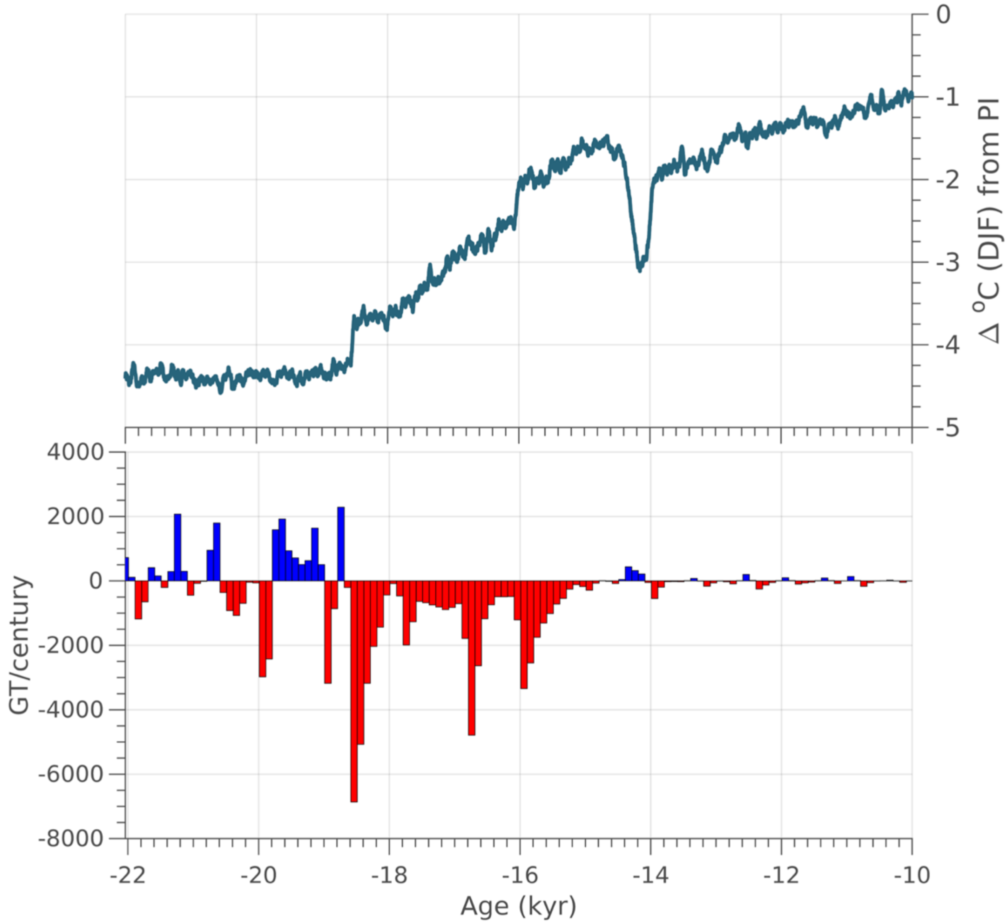

Figure 6. Top Panel: The TraCE-21ka Summer (DJF) temperature anomaly taken as the difference from the preindustrial period, area averaged across our model domain. Bottom Panel: The simulated ice mass change calculated in GT/century across the last deglaciation (22 ka to 10 ka). Red indicates ice mass loss, and blue indicates ice mass gain.

By 17 ka, the northern portion of the model domain (north of 39.5°S), has generally become ice free for the exception of the highest terrain (e.g., mountain glaciers). By 16 ka, between 39.5°S and 40.5°S, ice remains only on the highest terrain (Figure 5), however ice cover persists south of 40.5°S. Between 16 ka and 15 ka, summer temperature rises ~0.5°C (Figure 6) and the remaining ice sheet retreats south of 40.5°S. By 15 ka, there is no evidence of an ice sheet, with only mountain glaciers and small ice caps (e.g. Cerro Tronador) existing across the high terrain throughout the model domain (Figure 5).

After 15 ka, TraCE-21ka simulates a short and abrupt Antarctic Cold Reversal (ACR) between 14.6 ka and 14 ka (Figure 6), before temperatures continue to rise into the early Holocene. There is only a minor ice mass gain (e.g., <500 GT/yr) during the ACR, and minimal fluctuation in ice mass after 14 ka. By 10 ka, only small mountain glaciers persist across the high terrain and volcanoes of the CLD (gray color in Figure 5).

3.2.2 Sensitivity Tests

To better assess how changes in precipitation may modulate the deglaciation across the CLD we perform additional sensitivity tests. We refer to the simulation discussed above as our *main simulation*, where the climate boundary conditions of temperature and precipitation varied temporally and spatially across the last deglaciation. Three more simulations are performed where temperature is allowed to vary across the last deglaciation, but precipitation remains fixed at a given magnitude for a particular time interval. Each experiment is listed below as:

1) Monthly precipitation is held constant at the preindustrial mean. Preindustrial precipitation is reduced compared to the period 22 ka to18 ka, but is similar to and higher than what is simulated after 18 ka for the exception of the ACR at 14.5 ka (Figure 7).
2) Monthly precipitation is held constant at the 12.5 ka-12 ka mean. This is a period of reduced precipitation relative to the preindustrial (~7% reduction; Figure 7).
3) Monthly precipitation is held constant to the 22-20 ka mean, which is approximately 10% higher than preindustrial values across the Northern portion of the model domain (North of 40°S).

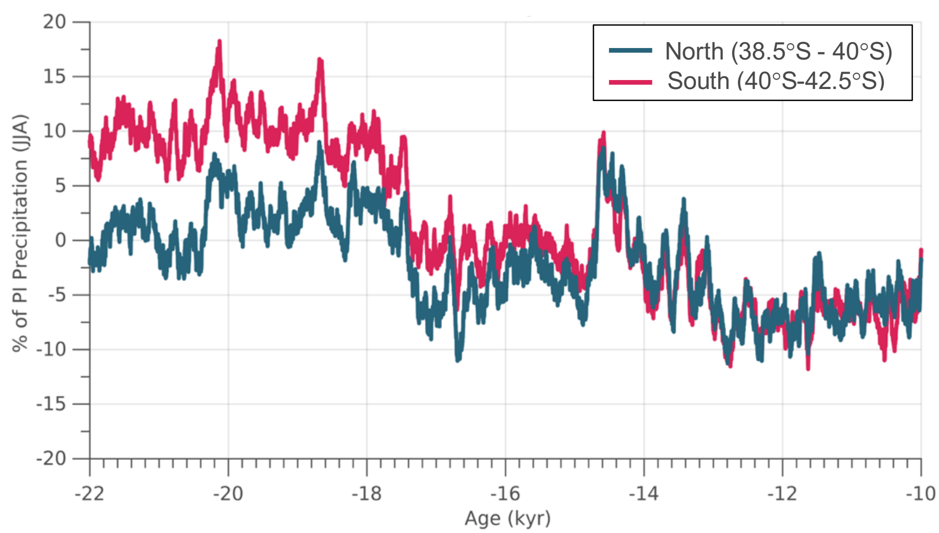

Figure 7. The winter (JJA) precipitation anomaly expressed as the percent difference from the preindustrial period. The area averaged anomaly is shown for the region north of 40°S and for the region south of 40°S (see Figure 2 for reference to the latitudinal range of our model domain).

Across our model domain during experiment 2 (Figure 8A), wintertime precipitation during the preindustrial is reduced compared to the early deglaciation (22 ka to 18ka) and is similar to slightly higher particularly south of 40°S after 18 ka (Figure 7). When holding precipitation constant at the preindustrial mean through the last deglaciation, the ice retreats faster across most portions of the model domain, particularly along the ice margins and in area north of 40°S. In the southern portion of our model domain (south of 40°S), where the changes in deglacial precipitation relative to the preindustrial are lower (Figure 7), the difference in simulated deglaciation age are also smaller. In general, the pace of deglaciation increases by up to 1 kyr compared to the main simulation, with many locations experiencing deglaciation 200-600 yrs earlier than the main simulation.

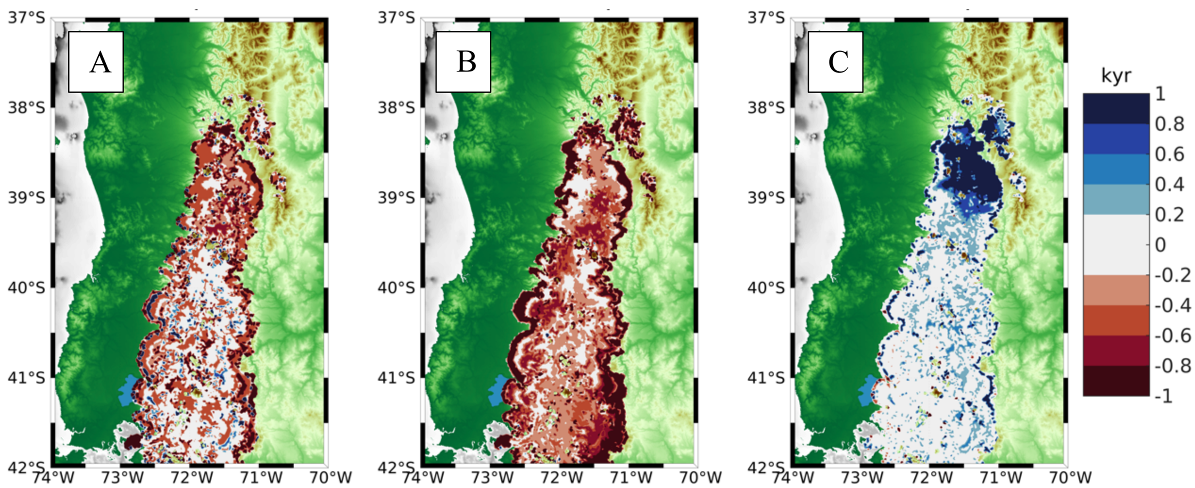

Figure 8. A) The difference in the simulated deglaciation age between sensitivity experiment 2 B.) experiment 3, C.) and experiment 4, from the main simulation. Blue colors indicate slower ice retreat for the sensitivity experiments compared to the main simulation, while red colors indicate faster ice retreat for the sensitivity experiments compared to the main run.

For our other two sensitivity tests, winter precipitation is reduced by up to 7% (Figure 8B) relative to the preindustrial across the model domain (Figure 7) and increased by up to 10% (Figure 8C) across the northern portion of the model domain (north of 40°S), but is similar to preindustrial values across the southern portion of our model domain (south of 40°S). For experiment 2 ice retreats faster across most of the CLD, along the ice margins and through the interior. Deglaciation along the margins occurs >1 kyr faster in many locations, and between 200 yrs to 1 kyr faster across portions of the ice interior. In experiment 3 with the imposed higher precipitation across the northern portion of the model domain, ice retreats slower during the last deglaciation relative to our standard simulation by >1 kyr, and in some locations up to 2 kyr.

3.3 Comparison to the reconstructed deglacial ice extent

Shown in Figure 1, PATICE assigns high to medium confidence to the reconstructed LGM (25 ka – 20 ka) ice extent along most of the western ice margin and portions of the eastern margin, with low confidence assigned to the northernmost ice extent. The majority of the ice history is poorly constrained (low confidence) during the deglaciation, and PATICE reconstructs a small cap that persists across the southern CLD until 10 ka, after which the ice disappears and only the Cerro Tronador glacier remains (see Figure 13 from Davies et al., 2020). We show the simulated and reconstructed ice extent in Figure 9 as well as the calculated ice area from PATICE at 20 ka, 15 ka, 13 ka, and 10ka and for our transient simulation in Figure 10. At 22 ka (Figure 9), our model simulates a generally greater ice extent along the eastern and western margin, except at the Seno de Reloncaví, Golfo de Ancud, and Lago Llanquihue, where the simulated ice margin does not advance to the well dated terminal LGM moraines (Mercer, 1972; Porter, 1981; Andersen et al., 1999; Denton et al., 1999). At 20 ka, the simulated ice area is 4.1×10^4 km^2 which is nearly identical to the PATICE areal extent across our model domain (Figure 10). The ice margin at the Seno de Reloncaví, Lago Llanquihue, and other locations along the eastern boundary in the CLD advances slightly at 20 ka, but still remain inboard of the PATICE reconstruction for these regions.

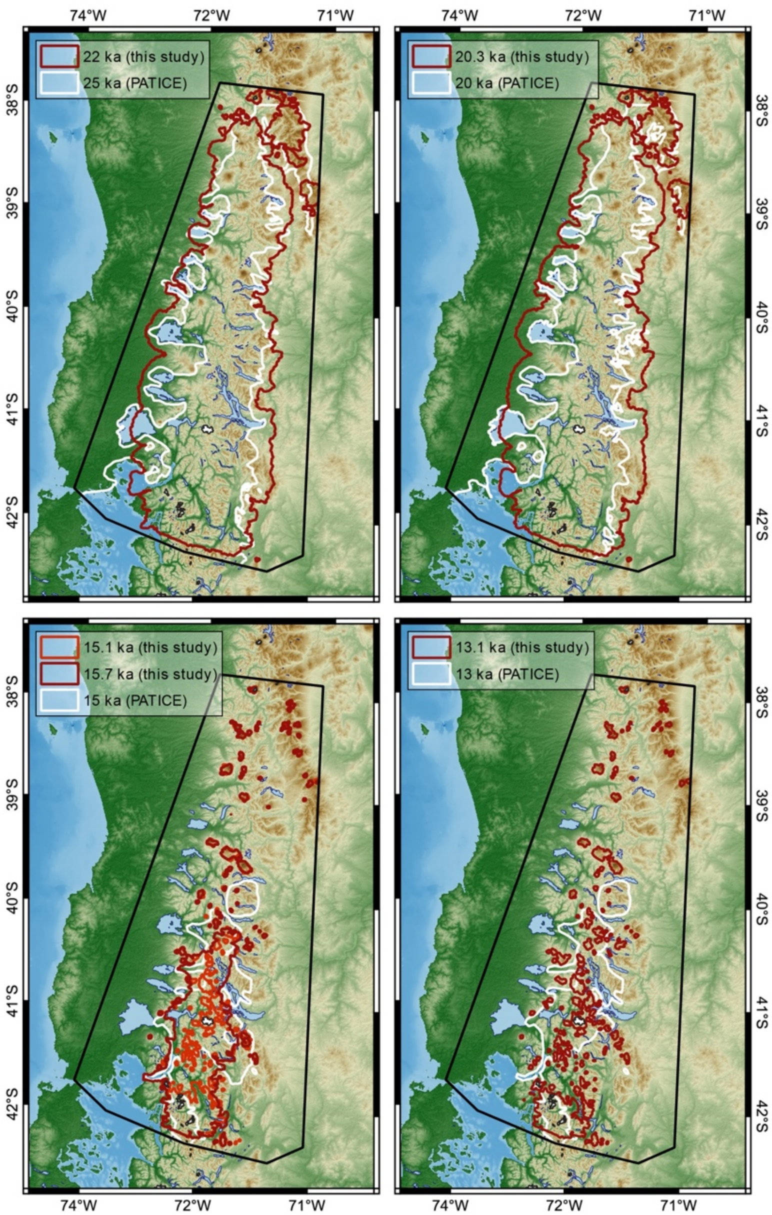

Figure 9. Comparison between the simulated ice extent at time intervals closest to the corresponding reconstructed ice extent from PATICE (Davies et al., 2020).

Between 18.3 ka and 15 ka large scale ice retreat occurs, and the simulated ice sheet loses 90% of its ice area, while the PATICE reconstruction suggests a reduction of 75% (Figure 10). At 15 ka, PATICE reconstructs an existing ice cap that separates from the remainder of the PIS to the south (Figure 9). This is in contrast to the simulated ice extent, which shows that by 15 ka, the PIS across our model domain has completely retreated and only mountain glaciers or small ice caps exist amongst the high terrain. However, if we compare the PATICE area at 15 ka and the simulated ice area at 15.7 ka (Figure 10), they are nearly identical at 1.2×10^4 km^2. While the PATICE ice extent at 15 ka and the simulated ice extent 15.7 ka do not match completely, the simulated ice extent at 15.7 ka still has evidence of a large ice cap similar to the PATICE reconstruction. Therefore, the simulated transition from ice sheet to ice cap and to discrete mountain glaciers occurs between 15.7 ka and 15 ka in our simulations. By 13 ka, our simulated ice area is 60% lower than the PATICE reconstructed area. By 10 ka this difference is 50%, however by this time the majority of the ice sheet has deglaciated (Figure 10), with our model simulating discrete mountain glaciers while PATICE reconstructs a small and narrow ice cap across the high terrain in the southern CLD (also see Figure 1).

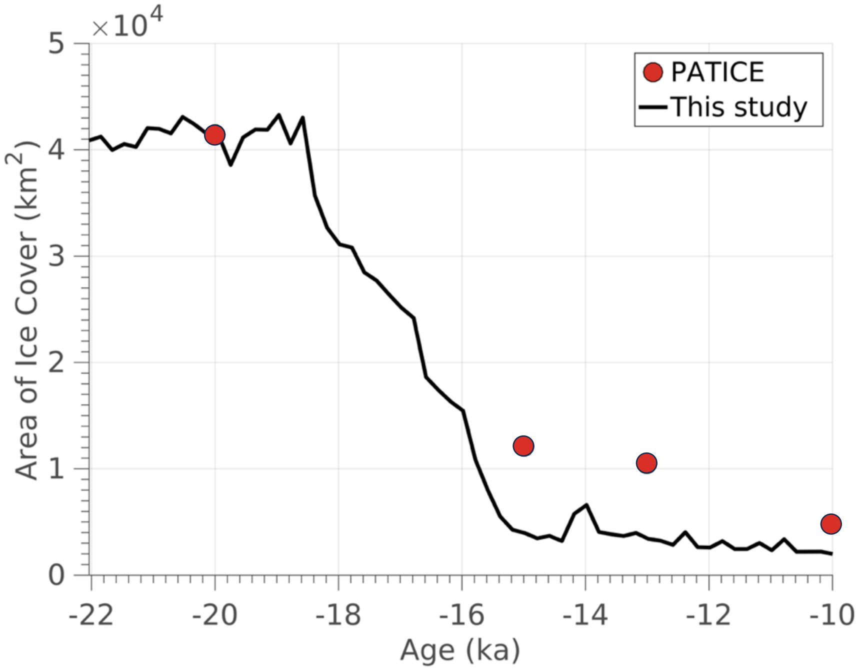

Figure 10. The simulated ice area (km^2) from 22 ka to 10 ka shown as the black line. The red dots indicate the calculated ice area across our model domain for the reconstructed ice extent from PATICE (Davies et al., 2020).

4 Discussion

4.1 Climate-ice sensitivity

Determining the influence of the SWW on the heat and hydrologic budget across South America during the LGM and last deglaciation remains difficult, as limitations in paleo-proxy data and disagreement between climate models prohibit certainty (Kohfeld, 2013; Berman et al., 2018). And while evidence does suggest wetter conditions across the CLD during the late glacial (Moreno and Videla, 2018), linking the paleoclimate change in SWW position and strength from regional paleoclimate proxies remains problematic (Kohfeld et al., 2013).

The scale at which we deduce ice history and climate interactions is also important. Looking at the PIS as a whole, recent numerical ice sheet modelling studies indicate that the simulated ice extent and volume for the entire PIS at the LGM is largely controlled by the magnitude of the temperature anomaly compared to present day (Yan et al., 2022). However, regional scale ice flow modelling informed by geologic constraints on past ice margin extent show that higher precipitation during the LGM (Leger et al., 2021), the late glacial, and the Holocene (Muir et al., 2023; Martin et al., 2022) is needed to support model-data agreement. It appears that during the LGM a northward shift in the SWW (Kohfeld et al., 2013; Rojas et al., 2009; Togweillier et al., 2006) or a strengthening or expansion of the wind belt (Lamy et al., 2010) is perhaps the most likely scenario, with high frequency variability possible during the deglaciation as atmospheric reorganization altered the heat and hydrologic budget as recorded by glacier and ice sheet change (Davies et al., 2020; Boex et al., 2013).

We analyzed outputs of the wintertime (JJA) 925 hPa zonal wind as the mean over 500 yr periods from TraCE-21ka for the LGM (22-21ka), 18ka (18.5-18ka), 16ka (16.5-16ka), 14ka (14.5-14ka), 12ka (12.5-12ka) and the Preindustrial (Supplemental section 3, Figures S3 A-E). Across our model domain and to its south, relative to the PI, zonal winds are stronger during the LGM with a southerly displacement (Figure S3A first and second column). During 18ka (Figure S3B), the zonal wind increases in strength relative to the PI, with the stronger winds having wider latitudinal coverage, particularly across our model domain. While the mean position of the SWW is poleward at 18ka relative to the PI (Jiang and Yan, 2022), across Patagonia the simulated position of the maximum zonal wind is at the same latitudinal band as the PI. At 16ka, the zonal wind is stronger across our domain and Patagonia (Figure S3C) relative to the PI, although not as large as the differences during 18ka. By 14ka, the strength in the zonal winds across Patagonia and our model domain are similar to slightly stronger than the PI (Figure S3D), however, the zonal wind maximum is situated more equatorward across our model domain relative to the PI. By 12ka (Figure S3E), the zonal wind is similar to slightly weaker than the PI across our model domain, although it is stronger relative to the PI to the south of our model domain across central and southern Patagonia. The position of the maximum zonal winds is also displaced further south relative to the PI. These changes in strength and position of the simulated SWW during the last deglaciation are similar to the findings of Jian and Yan (2020), which found that relative to the Preindustrial (PI), TraCE-21ka simulates a more poleward subtropical and subpolar jet over the Southern hemisphere at the LGM. During the remainder of the LGM and last deglaciation, the overall position of the SWW migrates northward in TraCE-21ka, with poleward displacements during Heinrich Stadial 1 (HS1), equatorward displacements during the Antarctic Cold Reversal (ACR), and poleward displacements during the Younger Dryas (YD), similar to our analysis.

Additionally, we evaluated the wintertime (JJA) low-level (850 hPa) moisture flux convergence from TraCE-21ka (MFC; Supplement section 4, Figure S4A-E), which is influenced by the mean flow and transient eddies in the extratropical hydrologic cycle (Peixoto and Oort, 1992). During the LGM and 18 ka, MFC increases across our model domain, consistent with a convergence of the mean flow moisture fields relative to the PI (Figure S4 A, B). During the LGM and 18ka, we note that TraCE-21ka simulates higher JJA precipitation anomalies (relative to the PI) across our model domain (Figure 7). While our analysis cannot directly constrain the source of the positive precipitation anomalies (e.g., mean flow, storms), the strength of the simulated SWW in TraCE-21ka increases across our model domain (Figure S3 A, B) coincident with the increases in MFC, which may contribute to the positive precipitation anomalies at these time intervals (Figure 7). By 16ka, there is increased divergence in the 925 hPa winds and moisture relative to the PI (Figure S4 C). Decreased MFC relative to the PI coincides with a reduction in precipitation across our model domain that is similar to or less than the PI (Figure 7). We note that the ice thickness boundary conditions used in the TraCE-21ka come from the Ice5G reconstruction (Peltier, 2004), which has the PIS being completely deglaciated by 16ka. However, our analysis cannot decompose whether the simulated changes in precipitation and MFC are a consequence of the coupling between regional atmospheric circulation and the ice thickness boundary conditions used in TraCE-21ka or if these changes represent wider interactions with changes in hemispheric atmospheric circulation. By 14ka, and during the ACR, MFC increases relative to the PI (Figure S4D). This is consistent with a simulated equatorward migration of the SWW as shown in Jiang and Yan (2020) and our analysis (Figure S3D), and positive anomalies in precipitation across our model domain relative to the PI (Figure 7). By 12ka, precipitation across our model domain is reduced relative to the PI (Figure 7), and TraCE-21ka simulates a reduction in the MFC as well as a poleward migration of the SWW (Figure S3E; Jiang and Yan, 2020).

When considering proxy records of precipitation across the CLD, there is reasonable agreement with the changes in precipitation simulated by TraCE-21ka. Moreno et al. (1999;2015) and Moreno and Videla (2018) find that wetter than present day conditions existed across the CLD during the LGM and early deglaciation which is consistent with the precipitation anomalies simulated by TraCE-21ka (Figure 7). These changes in paleoclimate proxies are attributed to an intensified storm track associated with an equatorward shift of the SWW (Moreno et al. 1999; 2015). While TraCE-21ka instead simulates a poleward shift of the SWW during these time intervals, increases in precipitation and the intensification of the storm track as inferred by Moreno et al. (2015) may also be consistent with a strengthening of the SWW as simulated by TraCE-21ka during these intervals (Figure S3 A, B; Rojas et al., 2009; Sime et al., 2013; Kohfeld et al., 2013). Moreno et al. (2015) note that rapid warming ensues across the CLD around 17,800 cal yr BP, which is similar to the timing of deglacial warming as simulated by TraCE-21ka around 18.5 ka (Figure 6). Coincident with this rapid temperature rise, Moreno et al. (2015) note a shift from hyper humid to humid conditions which aligns well with decreases in the simulated precipitation in TraCE-21ka across our model domain (Figure 7). Lastly, Moreno et al. (1999; 2015) find that colder and wetter conditions occur across the CLD during the ACR, and infer an equatorward expansion of the SWW as a potential cause. While TraCE-21ka simulates an abrupt and short ACR, it does simulate an equatorward expansion of the SWW (Figure S4 D; Jian and Yan, 2020), associated cooling (Figure 6), and increases in precipitation (Figure 7) that agree with the proxy data.

Prior numerical ice flow modelling has indicated that precipitation played an important role in controlling the extent of paleoglaciers across the PIS (Muir et al., 2023; Leger et al., 2021) by modulating the pace and magnitude of ice retreat and advance during deglaciation (Martin et al., 2022). Much of the TraCE-21ka simulated winter precipitation anomalies shown in Figure 7 are within 10% of the preindustrial value. The sensitivity tests conducted here suggest that modest changes (~10%) in precipitation can alter the pace of ice retreat across the CLD on timescales consistent with the resolution of geochronological proxies constraining past ice retreat. We note that while TraCE-21ka simulates variations in precipitation across our model domain that are consistent with hydroclimate proxies discussed above (Moreno et al., 1999; 2015; 2018), the magnitude of those changes is not as large as proxy data across the CLD indicate. For example, hydroclimate proxies suggest that the LGM and early deglaciation was up to 2 times wetter across the CLD than present day (Moreno et al., 1999; Heusser et al., 1999). Therefore, we can deduce from our sensitivity analysis here that higher precipitation anomalies during the LGM and last deglaciation, forced by proposed changes in the SWW (Moreno et al.,1999;2015), may have helped offset melt from deglacial warming thereby influencing the pacing of early deglacial ice retreat in this region.

4.2 Ice retreat during the Last Deglaciation

The PATICE dataset (Davies et al., 2020) serves as the best available reconstruction of ice margin change for the PIS across the last deglaciation. This state-of-the-art compilation provides an empirical reconstruction of the configuration of the PIS as isochrones every 5 ka, from 35 ka to present, based on detailed geomorphological data and available geochronological evidence. Because geochronological constraints on past PIS change are limited, the PATICE reconstruction assigns qualitative confidence to its reconstructed ice margins. Where there is agreement between geochronological and geomorphological indicators of past ice margin history (i.e., moraines), high confidence is assigned. Where geomorphological evidence suggests the existence of past ice margins, but lacks a geochronological constraint, medium confidence is assigned. Lastly, low confidence is assigned where there is a lack of any indicators of past ice sheet extent, where the ice limits result in interpolated interpretations from immediately adjacent moraines from valleys that have been mapped and dated. Across the CLD, the LGM ice extent is well constrained by geologic proxies particularly in the west and southwest (Figure 1). The moraines that constrain the piedmont ice lobes that formed along the western boundary are now presently lakes and have reasonable age control (Denton et al., 1999; Moreno et al., 1999; Lowell et al., 1995), giving confidence to the LGM ice margin limits. Beyond this region, age control is sparse along the western boundary for the timing of LGM ice extent, but the existence of well-defined moraines along lakes in the northern CLD are assumed to be in sync with those moraines deposited to the south (Denton et al., 1999). However, low confidence remains in the geologic reconstruction of the LGM ice boundary along the eastern margin where little to no chronological constraints are available. In general, deglaciation from the maximum LGM ice extent begins between 18 – 19 ka (Davies et al., 2020), however, poor age control and a lack of geomorphic indicators make it difficult to constrain the ice extent across this region during the deglaciation. For instance, a single cosmogenic nuclide surface exposure date retrieved from the Nahuel Huapi moraine yielded an age of ~31.4 ka (Zech et al., 2017). While it is assumed that the ice limit behaved similarly both to the west and east, the limited existing data prevents a comprehensive understanding of the ice extent at the northeastern margin. This induces the highest level of uncertainty in the reconstruction and hinders our data model comparison. Therefore, we rely on the PATICE dataset interpolated isochrones (low confidence) for this northeastern region as the state-of-the-art reconstruction.

In regards to ice area and extent, our simulated ice sheet at the LGM using TraCE-21ka climate boundary conditions agrees well with the PATICE reconstruction (Figure 10). Our simulations reveal that deglaciation began between 19 ka to 18 ka, consistent with the geologic proxies (Davies et al., 2020). The simulated ice retreat continues until 15 ka, with the largest pulses in ice mass loss occurring at 18.6 ka, 16.8 ka, and 16 ka (Figure 6). Where PATICE estimates an ice cap around 15 ka (~40°S), our simulations reveal that glaciation was restricted to high elevations. After 15 ka, mountain glaciers remain in our simulation but there is no presence of a large ice cap as reconstructed in PATICE. Comparison between the model simulations and PATICE becomes difficult during the 15 -13 ka period as confidence in the geologic reconstruction is low. Therefore, our model results offer a different reconstruction to PATICE, and indicate that the ice sheet in this region largely retreated by 15 ka, with only mountain glaciers remaining. However, during this interval, the Antarctic Cold Reversal (ACR) may have influenced the heat and hydrologic budget across this region, with wetter and cooler conditions interrupting the deglacial warming (Moreno et al., 2018). While TraCE-21ka simulates a cooler and wetter ACR, it is short-lived, lasting about 500 years as compared to 2,000 years in some ice core records or proxy-based studies (Lowry et al., 2019; He et al., 2013, Pedro et al., 2015). This potential for a favorable and prolonged period of glacier growth is likely missing in our simulations during the ACR, which may explain some of the mismatch against the PATICE reconstruction at 15 ka – 13 ka.

4.3 Limitations

Currently ISSM is undergoing model developments to include a full treatment of solid earth-ice and sea-level feedbacks (Adhikari et a., 2016). Therefore, at this time, there is no coupling between the ice sheet and solid earth. Instead, we prescribed GIA from a global GIA model of the last glacial cycle from Caron et al. (2018). While this model reasonably estimates GIA across the PIS over the last deglaciation, our simulated ice history does not feedback onto GIA. The ice history for Patagonia incorporated into the Caron et al. (2018) ensemble is from Ivins et al. 2011. Therefore, the prescribed GIA response across our domain does not perfectly match our simulated ice history. Additionally, the global mantle from Caron et al. (2018) does not exhibit regional low viscosity that is attributable to Patagonia and therefore, current rates of deformation are likely underestimated by the model. By not simulating the 2-way coupled ice and solid-earth interactions, we could be missing some feedbacks between our simulated ice history and the solid earth that may modulate the deglaciation across this region. Despite this limitation however, our prescribed GIA from Caron et al. (2018) is reasonable when compared with reconstructed deglacial GIA in Patagonia (Troch et al., 2022), giving confidence that our simulation is capturing the regional influence of GIA on the simulated ice history.

Across most of our domain, there is evidence for an advance of piedmont glaciers across glacial outwash during the LGM, which formed the physical boundary for some of the existing terminal moraines around the lakes within the CLD (Bentley, 1996; Bentley, 1997). The formation of ice-contact proglacial lakes likely occurred as a function of deglacial warming and ice retreat (Bentley, 1996). Where there were proglacial lakes along the westward ice front in the CLD, evidence suggests that ice was grounded during the LGM (Lago Puyehue; Heirman et al., 2011). During deglaciation, iceberg calving into the proglacial lakes may have occurred (Bentley 1996,1997; Davies et al., 2020), with evidence suggesting that local topography and calving may have controlled the spatially irregular timing of abandonment from the terminal moraines surrounding the proglacial lakes (Bentley, 1997). Recent glacier modelling (Sutherland et al., 2020) suggests that inclusion of ice-lake interactions may have large impacts on the magnitude and rate of simulated ice front retreat, as ice-lake interactions promote greater ice velocities, ice flux to the grounding line, and surface lowering. However, across our region, Heirman et al. (2011) indicate that it is not well constrained how the proglacial lakes in the CLD may have influenced local deglaciation, as more geomorphic data is needed. Therefore, because the inclusion of ice-lake interactions is relatively novel for numerical ice flow modeling (Sutherland et al., 2020; Quiquet et al., 2021; Hinck et al., 2022), we choose to not simulate the evolution and influence of proglacial lakes on the deglaciation across this model domain. Given this limitation, our simulated magnitude and rate of ice retreat at the onset of deglaciation may be underestimated, especially when looking at local deglaciation along these proglacial lakes. Although we do not think that these processes would greatly influence our conclusions regarding the role of climate on the evolution of the PIS is the CLD and the simulated ice retreat history, future work is required to assess the influence of proglacial lakes in this region.

5 Conclusions

In this study, we use a numerical ice sheet model to simulate the LGM and deglacial ice history across the northernmost extent of the PIS, the CLD. The ice sheet model used inputs of temperature and precipitation from the TraCE-21ka climate model simulation covering the last 22,000 years in order to simulate the deglaciation of the PIS across the CLD into the early Holocene.

Our numerical simulation suggests that large scale ice retreat occurs after 19 ka coincident with rapid deglacial warming, with the northern portion of the CLD becoming ice free by 17 ka. The simulated ice retreat agrees well with the most comprehensive geologic assessment of past PIS history available (PATICE; Davies et al., 2020) for the LGM ice extent and early deglacial but diverge when considering the ice geometry at and after 15 ka. In our simulations, the PIS persists until 15 ka across the remainder of the CLD, followed by ice retreat to higher elevations as mountain glaciers and small ice caps persist into the early Holocene (e.g., Cerro Tronador). The geologic reconstruction from PATICE instead estimates a small ice cap persisting across the southern portion of high terrain in the CLD until about 10 ka. However, of the limited geologic constraints particularly after 15 ka, high uncertainty in the timing and extent of deglacial ice history remains in the geologic reconstruction. Therefore, our results provide an additional reconstruction of the deglaciation of the PIS across the CLD that differs from PATICE after 15 ka, emphasizing a need for future work that aims to improve geologic reconstructions of past ice margin migration particularly during the later deglaciation across this region.

While deglacial warming was a primary driver of the demise of the PIS across the last deglaciation, we find that precipitation modulates the pacing and magnitude of deglacial ice retreat across the CLD. Paleoclimate proxies within the CLD has shown that the strength and position of the SWW varied during the LGM and last deglaciation, altering hydrologic patterns and influencing the deglacial mass balance. We find that the simulated changes in the strength and position of the SWW in TraCE-21ka are similar to those inferred from paleoclimate proxies of precipitation, consistent with a wetter than preindustrial climate being simulated and reconstructed over the CLD and in particular the region north of 40°S. Through a series of sensitivity tests, we alter the magnitude of the precipitation anomaly modestly (up to 10%) during our transient deglacial simulations and find that the pacing of ice retreat can speed up or slow down by a few hundred years and up to 2000 years depending on the imposed increase or decrease in the precipitation anomaly. While paleoclimate proxies of precipitation suggest that the CLD may have experienced twice as much precipitation during the LGM and early deglacial relative to present day (Moreno et al.,1999;2015), TraCE-21ka simulates smaller increases in LGM and early deglacial precipitation (~10-15% greater than preindustrial). Therefore, while our modelling suggests that modest changes in precipitation can modulate the pace of deglacial ice retreat across the CLD, from our analysis we can deduce that larger anomalies in precipitation as found in the paleoclimate proxies may have an even larger impact on modulating deglacial ice retreat. Because paleoclimate proxies of past precipitation are often lacking, and climate models can simulate a range of possible LGM and deglacial hydrologic states, these results suggest that improved knowledge of the past precipitation is critical towards better understanding the drivers of PIS growth and demise, especially as small variations in precipitation can modulate ice sheet history on scales consistent with geologic proxies.

Code/Data Availability

The simulations performed for this paper made use of the open-source Ice-Sheet and Sea-level System Model (ISSM) and are publicly available at https://issm.jpl.nasa.gov/ (Larour et al., 2012).

Author Contribution

JC and SM secured funding for this research. JC, MR, and SM all contributed to the project design. JC performed the model setup and simulations. JC performed the analyses on model output, with help from MR who performed analysis on PATICE reconstructions. JC wrote the manuscript with input from MR and SM.

Competing interests

The contact author has declared that none of the authors has any competing interests.

Acknowledgements

This work was supported by a grant from the National Science Foundation, Frontier Research in Earth Sciences # 2121561. We would like to thank Lambert Caron from the Jet Propulsion Laboratory for his input regarding Glacial Isostatic Adjustment across our study region.

References

Adhikari, S., Ivins, E. R., and Larour, E., 2016, ISSM-SESAW v1.0: mesh-based computation of gravitationally consistent sea level and geodetic signatures caused by cryosphere and climate driven mass change, Geoscientific Model Development, 9, 9769-9816, doi: 10.5194/gmd-9-1087-2016.

Åkesson, H., Morlighem, M., Nisancioglu, K. H., Svendsen, J. J., and Mangerud, J.: Atmosphere-driven ice sheet mass loss paced by topography: Insights from modelling the south-western Scandinavian Ice Sheet. 2018. Quaternary Sci. Rev., 195, 32–47, https://doi.org/10.1016/j.quascirev.2018.07.004.

Andersen, B., Denton, G. H., & Lowell, T. V. (1999). Glacial geomorphologic maps of Llanquihue drift in the area of the southern Lake District, Chile. Geografiska Annaler: Series A, Physical Geography, 81(2), 155-166.

Bentley, M.J., 1996. The role of lakes in moraine formation, Chilean Lake District. Earth Surf. Process. Landf. 21, 493–507. https://doi.org/10.1002/(SICI)1096-9837(199606)21:6<493::AID-ESP612>3.0.CO;2-D

Bentley, M.J., 1997. Relative and radiocarbon chronology of two former glaciers in the Chilean Lake District. J. Quat. Sci. 12, 25–33. https://doi.org/10.1002/(SICI)1099-1417(199701/02)12:1<25::AID-JQS289>3.0.CO;2-A

Berman, L., Silvestri, G., Tonello, M.S., On differences between Last Glacial Maximum and Mid-Holocene climates in southern South America simulated by PMIP3 models. 2018. Quat. Sci. Rev. 185. 113-121. https://doi.org/10.1016/j.quascirev.2018.02.003.

Blatter, H.: Velocity and stress-fields in grounded glaciers: A simple algorithm for including deviatoric stress gradients. 1995. J. Glaciol., 41, 333-344, https://doi.org/10.3189/S002214300001621X

Boex, J., Fogwill, C., Harrison, S. et al. Rapid thinning of the late Pleistocene Patagonian Ice Sheet followed migration of the Southern Westerlies. 2013. Sci Rep **3**, 2118. https://doi.org/10.1038/srep02118

Boisier, J. P., Alvarez-Garretón, C., Cepeda, J., Osses, A., Vásquez, N., and Rondanelli, R.: CR2MET: A high-resolution precipitation and temperature dataset for hydroclimatic research in Chile. 2018. EGUGA, p. 19739.

Braun, M.H., Malz, P., Sommer, C., Far.as-Barahona, D., Sauter, T., Casassa, G., Soruco, A., Skvarca, P., Seehaus, T.C., 2019. Constraining glacier elevation and mass changes in South America. Nat. Clim. Chang. 9, 130–136. https://doi.org/10.1038/s41558-018-0375-7

Brierley, C. M., Zhao, A., Harrison, S. P., Braconnot, P., Williams, C. J. R., Thornalley, D. J. R., Shi, X., Peterschmitt, J.-Y., Ohgaito, R., Kaufman, D. S., Kageyama, M., Hargreaves, J. C., Erb, M. P., Emile-Geay, J., D'Agostino, R., Chandan, D., Carré, M., Bartlein, P. J., Zheng, W., Zhang, Z., Zhang, Q., Yang, H., Volodin, E. M., Tomas, R. A., Routson, C., Peltier, W. R., Otto-Bliesner, B., Morozova, P. A., McKay, N. P., Lohmann, G., Legrande, A. N., Guo, C., Cao, J., Brady, E., Annan, J. D., and Abe-Ouchi, A.: Large-scale features and evaluation of the PMIP4-CMIP6 *midHolocene* simulations, Clim. Past, 16, 1847–1872, https://doi.org/10.5194/cp-16-1847-2020, 2020.

Briner, J. P., Cuzzone, J. K., Badgeley, J. A., Young, N. E., Steig, E. J., Morlighem, M., Schlegel, N.-J., Hakim, G., Schaefer, J. Johnson, J. V., Lesnek, A. L., Thomas, E. K., Allan, E., Bennike, O., Cluett, A. A., Csatho, B., de Vernal, A., Downs, J., Larour, E., and Nowicki, S.: Rate of mass loss from the Greenland Ice Sheet will exceed Holocene values this century. 2020. Nature, 6, 70–74, https://doi.org/10.1038/s41586-020-2742-6.

Bondzio, J. H., Seroussi, H., Morlighem, M., Kleiner, T., Rückamp, M., Humbert, A., and Larour, E. Y.: Modelling calving front dynamics using a level-set method: application to Jakobshavn Isbræ, West Greenland. 2016. The Cryosphere, 10, 497–510, https://doi.org/10.5194/tc-10-497-2016

Budd. W.F., P. L. Keage, N. A. Blundy. Empirical studies of ice sliding. 1979. J. Glaciol., 23:157-170.

Caron, L., Ivins, E. R., Larour, E., Adhikari, S., Nilsson, J., and Blewitt, G.: GIA model statistics for GRACE hydrology, cryosphere and ocean science. 2018. Geophys. Res. Lett., 45, 2203–2212, https://doi.org/10.1002/2017GL076644

Choi, Y., Morlighem, M., Rignot, E., and Wood, M.: Ice dynamics will remain a primary driver of Greenland ice sheet mass loss over the next century. 2021. Commun. Earth Environ., 2, 26, https://doi.org/10.1038/s43247-021-00092-z

Clark, P.U., He, F., Golledge, N.R., Mitrovica, J.X., Dutton, A., Hoffman, J.S., and Dendy, S., 2020, Oceanic forcing of penultimate deglacial and last interglacial sea-level rise: Nature, v. 577, p. 660–664, doi:10.1038/s41586-020-1931-7.

Cuffey, K. M. and Paterson, W. S. B.: The physics of glaciers, 4th edn. 2010. Butterworth-Heinemann, Oxford, ISBN 9780123694614

Cuzzone, J. K., Schlegel, N.-J., Morlighem, M., Larour, E., Briner, J. P., Seroussi, H., and Caron, L.: The impact of model resolution on the simulated Holocene retreat of the southwestern

Greenland ice sheet using the Ice Sheet System Model (ISSM). 2019. The Cryosphere, 13, 879–893, https://doi.org/10.5194/tc-13-879-2019.

Cuzzone, J. K., Young, N. E., Morlighem, M., Briner, J. P., and Schlegel, N.-J.: Simulating the Holocene deglaciation across a marine-terminating portion of southwestern Greenland in response to marine and atmospheric forcings. 2022. The Cryosphere, 16, 2355–2372, https://doi.org/10.5194/tc-16-2355-2022.

Davies, B.J., Darvill, C.M., Lovell, H., Bendle, J.M., Dowdeswell, J.A., Fabel, D., Gheorghiu, D.M., 2020. The evolution of the Patagonian ice sheet from 35 ka to the present day (PATICE). Earth Sci. Rev. 204, 103152. https://doi.org/10.1016/ j.earscirev.2020.103152.

Darvill., C.M., Stokes, C.R., Bentley, M.J., Evans, D.J.A., Lovell, H. 1996. Dynamics of former ice lobes of the southernmost Patagonian Ice Sheet based on glacial landsystems approach. Journal of Quaternary Science. 32, 6, 857-876. https://doi.org/10.1002/jqs.2890

Darvill, C.M., Stokes, C.R., Bentley, M.J., Evans, D.J.A., Lovell, H., Dynamics of former ice lobes of the southernmost Patagonian Ice Sheet based on glacial landsystems approach. 2017. J. Quaternary Sci., 32:857-876. https://doi.org/10.1002/jqs.2890

Denton, G.H., Lowell, T.V., Heusser, C.J., Schlüchter, C., Andersen, B.G., Heusser, L.E., Moreno, P.I., Marchant, D.R., 1999. Geomorphology, Stratigraphy, and Radiocarbon Chronology of LlanquihueDrift in the Area of the Southern Lake District, Seno Reloncav., and Isla Grande de Chilo., Chile. Geogr. Ann. Ser. A Phys. Geogr. 81, 167–229. https://doi.org/10.1111/1468-0459.00057

Denton, G.H., Heusser, J., Lowell, T.V., Moreno, P.I., Andersen, B.G., Heusser, L.E., Schlühter, C., Marchant, D.R. 1999. Interhemispheric Linkage of Paleoclimate During the Last Glaciation. Geografiska Annaler. 81, 2, 107-153. https://doi.org/10.1111/1468-0459.00055

Dias dos Santos, T., Morlighem, M., and Brinkerhoff, D.: A new vertically integrated MOno-Layer Higher-Order (MOLHO) ice flow model. 2022. The Cryosphere, 16, 179–195, https://doi.org/10.5194/tc-16-179-2022.

Díaz, C., Moreno, P. I., Villacís, L. A., Sepúlveda-Zúñiga, E. A., & Maidana, N. I. (2023). Freshwater diatom evidence for Southern Westerly Wind evolution since∼ 18 ka in northwestern Patagonia. Quaternary Science Reviews, 316, 108231.

Fernandez, A., Mark, B.G. 2016. Modeling modern glacier response to climate changes along the Andes Cordillera: A multiscale review, J. Adv. Model. Earth Syst., 8, 467–495, doi:10.1002/2015MS000482.

Garreaud, R., Lopez, P., Minvielle, M., & Rojas, M. (2013). Large-scale control on the Patagonian climate. Journal of Climate, 26(1), 215-230.

GEBCO Bathymetric Compilation Group 2021. 2021. The GEBCO_2021 Grid - a continuous terrain model of the global oceans and land. NERC EDS British Oceanographic Data Centre NOC. doi:10.5285/c6612cbe-50b3-0cff-e053-6c86abc09f8f

Glasser, N. F., Jansson, K. N., Harrison, S., & Kleman, J. (2008). The glacial geomorphology and Pleistocene history of South America between 38 S and 56 S. Quaternary Science Reviews, 27(3-4), 365-390.

Glen, J. W. The creep of polycrystalline ice. 1955. P. Roy. Soc. Lond. A, 228, 519–538, https://doi.org/10.1098/rspa.1955.0066.

Golledge, N. R., Thomas, Z. A., Levy, R. H., Gasson, E. G. W., Naish, T. R., McKay, R. M., Kowalewski, D. E., and Fogwill, C. J.: Antarctic climate and ice-sheet configuration during the early Pliocene interglacial at 4.23 Ma, Clim. Past, 13, 959–975, https://doi.org/10.5194/cp-13-959-2017, 2017.

Hajima, T., Watanabe, M., Yamamoto, A., Tatebe, H., Noguchi, M. A., Abe, M., Ohgaito, R., Ito, A., Yamazaki, D., Okajima, H., Ito, A., Takata, K., Ogochi, K., Watanabe, S., and Kawamiya, M.: Development of the MIROC-ES2L Earth system model and the evaluation of biogeochemical processes and feedbacks, Geosci. Model Dev., 13, 2197–2244, https://doi.org/10.5194/gmd-13-2197-2020

He, F., Shakun, J. D., Clark, P. U., Carlson, A. E., Liu, Z., Otto-Bliesner, B. L., Kutzbach, J. E. 2013. Northern Hemisphere forcing of Southern Hemisphere climate during the last deglaciation, Nature, 494, 81–85. doi: 10.1038/nature11822.

He, F., Clark, P.U. 2022. Freshwater forcing of the Atlantic Meridional Overturning Circulation revisited. Nature Climate Change. 12. 449-454. https://doi.org/10.1038/s41558-022-01328-2.

Heirman, K., De Batist, M., Charlet, F., Moernaut, J., Chapron, E., Brümmer, R., Pino, M., Urrutia, R., 2011. Detailed seismic stratigraphy of Lago Puyehue: implications for the mode and timing of glacier retreat in the Chilean Lake District. J. Quat. Sci. 26, 665–674. https://doi.org/10.1002/jqs.1491

Hinck, S., Gowan, E. J., Zhang, X., and Lohmann, G.: PISM-LakeCC: Implementing an adaptive proglacial lake boundary in an ice sheet model. 2022. The Cryosphere, 16, 941–965, https://doi.org/10.5194/tc-16-941-2022.

Hubbard, A., Hein, A.S., Kaplan, M.R., Hulton, N.R.J., Glasser, N., 2005. A modelling reconstruction of the last glacial maximum ice sheet and its deglaciation in the vicinity of the northern patagonian icefield, south America. Geogr. Ann. Phys.Geogr. 87 (2), 375-391. https://doi.org/10.1111/j.0435-3676.2005.00264.x

Hulton, N.R.J., Purves, R., McCulloch, R., Sugden, D.E., Bentley, M.J., 2002. The last glacial maximum and deglaciation in southern south America. Quat. Sci. Rev. 21 (1), 233-241. https://doi.org/10.1016/S0277-3791(01)00103-2.

Hulton, N., Sugden, D., Payne, A., Clapperton, C., 1994. Glacier modeling and the climate of Patagonia during the last glacial maximum. Quat. Res. 42 (1), 1-19. doi:10.1006/qres.1994.1049

Jiang, N., Yan, Q. Evolution of the meridional shift of the subtropical and subpolar westerly jet over the Southern Hemisphere during the past 21,000 years. 2020. Quat Sci. Rev. 246, https://doi.org/10.1016/j.quascirev.2020.106544.

Kilian, R., Lamy, F., 2012. A review of Glacial and Holocene paleoclimate records from southernmost Patagonia (49e55 S). Quat. Sci. Rev. 53, doi.10.1016/j.quascirev.2012.07.017

Kageyama, M., Harrison, S. P., Kapsch, M.-L., Lofverstrom, M., Lora, J. M., Mikolajewicz, U., Sherriff-Tadano, S., Vadsaria, T., Abe-Ouchi, A., Bouttes, N., Chandan, D., Gregoire, L. J., Ivanovic, R. F., Izumi, K., LeGrande, A. N., Lhardy, F., Lohmann, G., Morozova, P. A., Ohgaito, R., Paul, A., Peltier, W. R., Poulsen, C. J., Quiquet, A., Roche, D. M., Shi, X., Tierney, J. E., Valdes, P. J., Volodin, E., and Zhu, J. 2021. The PMIP4 Last Glacial Maximum experiments: preliminary results and comparison with the PMIP3 simulations, Clim. Past, 17, 1065–1089, https://doi.org/10.5194/cp-17-1065-2021.

Kilian, R., Lamy, F. A review of Glacial and Holocene paleoclimate records from southernmost Patagonia (49-55°S). 2012. 53, 15, 1-23. https://doi.org/10.1016/j.quascirev.2012.07.017

Kohfeld, K.E., Graham, R.M., Boer, A. M. de, Sime, L.C., Wolff, E.W., Qu er e, C.L., Bopp, L., 2013. Southern Hemisphere westerly wind changes during the Last Glacial Maximum: paleo-data synthesis. Quat. Sci. Rev. 68, 76-95. , 10.1016/j.quascirev.2013.01.017

Lamy, F., Kilian, R., Arz, H.W., Francois, J.-P., Kaiser, J., Prange, M., Steinke, T., 2010. Holocene changes in the position and intensity of the southern westerly wind belt.Nat. Geosci. 3, 695–699. https://doi.org/10.1038/ngeo959

Lamy, F., Arz, H. W., Kilian, R., Lange, C. B., Lembke-Jene, L., Wengler, M., ... & Tiedemann, R. (2015). Glacial reduction and millennial-scale variations in Drake Passage throughflow. Proceedings of the National Academy of Sciences, 112(44), 13496-13501 https://doi.org/10.1073/pnas.1509203112

Larour, E., Seroussi, H., Morlighem, M., and Rignot, E.: Continental scale, high order, high spatial resolution, ice sheet modeling using the Ice Sheet System Model (ISSM). 2012. J. Geophys. Res.-Earth, 117, F01022, https://doi.org/10.1029/2011JF002140

Le Morzadec, K., Tarasov, L., Morlighem, M., and Seroussi, H.: A new sub-grid surface mass balance and flux model for continental-scale ice sheet modelling: testing and last glacial cycle. 2015. Geosci. Model Dev., 8, 3199–3213, https://doi.org/10.5194/gmd-8-3199-2015

Leger TPM, Hein AS, Goldberg D,Schimmelpfennig I, Van Wyk de Vries MS, Bingham RG and ASTER Team (2021) Northeastern Patagonian Glacier Advances (43°S) Reflect Northward Migration of the Southern Westerlies Towards the End of the Last Glaciation. Front. Earth Sci. 9:751987. doi: 10.3389/feart.2021.751987

Liu, Z., Otto-Bliesner, B., He, F., Brady, E., Tomas, R., Clark, P., Carlson, A., Lynch-Stieglitz, J., Curry, W., Brook, E., Erickson, D., Jacob, R., Kutzbach, J., and Cheng, J. 2009. Transient simulation of last deglaciation with a new mechanism for Bølling-Allerød warming, Science, 325, 310–314. https://doi.org/10.1126/science.1171041

Lowry, D. P., Golledge, N. R., Menviel, L., and Bertler, N. A. N.: Deglacial evolution of regional Antarctic climate and Southern Ocean conditions in transient climate simulations. 2019. Clim. Past, 15, 189–215, https://doi.org/10.5194/cp-15-189-2019.

Lowell, T., Heusser, C., Andersen, B., Moreno, P., Hauser, A., Heusser, L., Schlüchter, C.,Marchant, D., Denton, G., 1995. Interhemispheric correlation of late Pleistoceneglacial events. Science 269, 1541–1549. Doi: 10.1126/science.269.5230.1541

Lowry, D. P., Golledge, N. R., Menviel, L., and Bertler, N. A. N.: Deglacial evolution of regional Antarctic climate and Southern Ocean conditions in transient climate simulations. 2019. Clim. Past, 15, 189–215, https://doi.org/10.5194/cp-15-189-2019

Marcott, S.A., Shakun, J.D., Clark, P.U., Mix, A.C. 2013. A Reconstruction of Regional and Global Temperature for the Past 11,300 Years. 339, 6124, 1198-1201. DOI: 10.1126/science.1228026

Martin J, Davies BJ, Jones R and Thorndycraft V (2022), Modelled sensitivity of Monte San Lorenzo ice cap, Patagonian Andes, to past and present climate. Front. Earth Sci. 10:831631. doi: 10.3389/feart.2022.831631

Mauritsen, T., Bader, J., Becker, T., Behrens, J., Bittner, M., Brokopf, R., Brovkin, V., Claussen, M., Crueger, T., Esch, M., Fast, I., Fiedler, S., Fläschner, D., Gayler, V., Giorgetta, M., Goll, D. S., Haak, H., Hagemann, S., Hedemann, C., Hohenegger, C., Ilyina, T., Jahns, T., Jimenéz-de-la-Cuesta, D., Jungclaus, J., Kleinen, T., Kloster, S., Kracher, D., Kinne, S., Kleberg, D., Lasslop, G., Kornblueh, L., Marotzke, J., Matei, D., Meraner, K., Mikolajewicz, U., Modali, K., Möbis, B., Müller, W. A., Nabel, J. E. M. S., Nam, C. C. W., Notz, D., Nyawira, S.-S., Paulsen, H. Peters, K., Pincus, R., Pohlmann, H. Pongratz, J., Popp, M., Raddatz, T. J., Rast, S., Redler, R., Reick, C. H., Rohrschneider, T., Schemann, V., Schmidt, H., Schnur, R., Schulzweida, U., Six, K. D., Stein, L., Stemmler, I., Stevens, B., von Storch, J.-S., Tian, F., Voigt, A., Vrese, P., Wieners, K.-H., Wilkenskjeld, S., Winkler, A., and Roeckner, E.: Developments in the MPI-M Earth System Model version 1.2 (MPI-ESM1.2) and its response to increasing CO_2, J. Adv. Model. Earth Syst. 2019. 11, 998–1038, https://doi.org/10.1029/2018MS001400

Meier, W.J-H., Grießinger, J., Hochreuther, P., Braun, M.H. 2018. An updated multi-temporal glacier inventory for the Patagonian Andes with changes between the Little Ice Age and 2016. Frontiers in Earth Science, 6, 62. https://doi.org/10.3389/feart.2018.00062

Menviel, L., A. Timmermann, A. Mouchet, and O. Timm, 2008: Climate and marine carbon cycle response to changes in the strength of the Southern Hemispheric westerlies. *Paleoceanography*, **23**, PA4201, doi:10.1029/2008PA001604.

Mercer, J.H., 1972. Chilean glacial chronology 20,000 to 11,000 carbon-14 years ago:some global comparisons. Science 176, 1118–1120. DOI: 10.1126/science.176.4039.1118

Moreno, P. I., Lowell, T. V., Jacobson Jr, G. L., & Denton, G. H. (1999). Abrupt vegetation and climate changes during the last glacial maximumand last termination in the chilean lake district: a case study from canal de la puntilla (41 s). Geografiska Annaler: Series A, Physical Geography, 81(2), 285-311.

Moreno, P.I., Denton, G.H., Moreno, H., Lowell, T.V., Putnam, A.E., Kaplan, M.R., 2015. Radiocarbon chronology of the last glacial maximum and its termination in northwestern Patagonia. Quat. Sci. Rev. 122, 233e249. 10.1016/j.quascirev.2015.05.027

Moreno, P.I., Videla, J., Valero-Garc es, B.L., Alloway, B.V., Heusser, L.E., 2018. A continuous record of vegetation, fire-regime and climatic changes in northwestern Patagonia spanning the last 25,000 years. Quat. Sci. Rev. 198, 10.1016/j.quascirev.2018.08.013

Morlighem, M., Bondzio, J., Seroussi, H., Rignot, E., Larour, E., Humbert, A., and Rebuffi, S.: Modeling of Store Gletscher's calving dynamics, West Greenland, in response to ocean thermal forcing. 2016. Geophys. Res. Lett., 43, 2659–2666, https://doi.org/10.1002/2016GL067695

Muir, R., Eaves, S., Vargo, L., Anderson, B., Mackintosh, A., Sagredo, E., Soteres, R. Late glacial climate evolution in the Patagonian Andes (44-47°S) from alpine glacier modelling. 2023. Quaternary Science Reviews, 305, https://doi.org/10.1016/j.quascirev.2023.108035.

Ohgaito, R., Yamamoto, A., Hajima, T., O'ishi, R., Abe, M., Tatebe, H., Abe-Ouchi, A., and Kawamiya, M.: PMIP4 experiments using MIROC-ES2L Earth system model, Geosci. Model Dev., 14, 1195–1217, https://doi.org/10.5194/gmd-14-1195-2021

Pattyn, F.: A new three-dimensional higher-order thermomechanical ice sheet model: Basic sensitivity, ice stream development, and ice flow across subglacial lakes. 2003. J. Geophys. Res., 108, 2382, https://doi.org/10.1029/2002JB002329

Pedro, J. B., Bostock, H. C., Bitz, C. M., He, F., Vandergoes, M. J., Steig, E. J., Chase, B.M., Krause, C.E., Rasmussen, S.O., Bradley, M.R., Cortese, G. 2016. The spatial extent and dynamics of the Antarctic Cold Reversal. Nature Geoscience, 9(1), 51-55. https://doi.org/10.1038/ngeo2580

Peixoto, J. P., and A. H. Oort (1992), Physics of Climate, American Institute of Physics, 520 pp.

Pfeffer, W.T., Arendt, A.A., Bliss, A., Bolch, T., Cogley, J.G., Gardner, A.S., Hagen, J.O., Hock, R., Kaser, G., Kienholz, C. and Miles, E.S. 2014. The Randolph Glacier Inventory: a globally complete inventory of glaciers. Journal of Glaciology, 60, 537-552. Doi:10.31.3189/2014JoG13J176

Pollard, D. and DeConto, R. M.: Description of a hybrid ice sheet-shelf model, and application to Antarctica. 2012. Geosci. Model Dev., 5, 1273–1295, https://doi.org/10.5194/gmd-5-1273-2012.

Porter, S. C. (1981). Pleistocene glaciation in the southern Lake District of Chile. Quaternary Research, 16(3), 263-292.

Quiquet, A., Dumas, C., Paillard, D., Ramstein, G., Ritz, C., and Roche, D. M.: Deglacial Ice Sheet Instabilities Induced by Proglacial Lakes. 2021. Geophys. Res. Lett., 48, e2020GL092141, https://doi.org/10.1029/2020GL092141

Rojas, M., Moreno, P., Kageyama, M., Crucifix, M, Hewitt, C., Abe-Ouchi, A., Ohgaito, R., Brady, E.C., Hop, P. 2009. The Southern Westerlies during the last glacial maximumin PMIP2 simulations. Clim. Dyn. 32, 525–548. https://doi.org/10.1007/s00382-008-0421-7.

Rojas, M., 2013. Sensitivity of southern Hemisphere circulation to LGM and 4 CO_2 climates. Geophys. Res. Lett. 40, 965e970.

Sepulchre, P., Caubel, A., Ladant, J.-B., Bopp, L., Boucher, O., Braconnot, P., Brockmann, P., Cozic, A., Donnadieu, Y., Dufresne, J.-L., Estella-Perez, V., Ethé, C., Fluteau, F., Foujols, M.-A., Gastineau, G., Ghattas, J., Hauglustaine, D., Hourdin, F., Kageyama, M., Khodri, M., Marti, O., Meurdesoif, Y., Mignot, J., Sarr, A.-C., Servonnat, J., Swingedouw, D., Szopa, S., and Tardif, D.: IPSL-CM5A2 – an Earth system model designed for multi-millennial climate simulations, Geosci. Model Dev., 2020. 13, 3011–3053, https://doi.org/10.5194/gmd-13-3011-2020

Seguinot, J., Rogozhina, I., Stroeven, A. P., Margold, M., and Kleman, J.: Numerical simulations of the Cordilleran ice sheet through the last glacial cycle, The Cryosphere, 10, 639–664, https://doi.org/10.5194/tc-10-639-2016, 2016.

Shakun, J., Clark, P., He, Marcott, S.A., Mix, A. C., Liu, A., Otto-Bliesner, B., Schmittner, A., Bards, E. 2012. Global warming preceded by increasing carbon dioxide concentrations during the last deglaciation. *Nature* 484, 49–54. https://doi.org/10.1038/nature10915

Shakun, J.D., Lea, D.W., Lisiecki, L.E., Raymo, M.E. 2015. An 800-kyr record of global surface ocean $\delta^{18}O$ and implications for ice volume-temperature coupling. 426, 58-68. https://doi.org/10.1016/j.epsl.2015.05.042

Sidorenko, D., Goessling, H., Koldunov, N., Scholz, P., Danilov, S., Barbi, D., Cabos, W., Gurses, O., Harig, S., Hinrichs, C., Juricke, S., Lohmann, G., Losch, M., Mu, L., Rackow, T., Rakowsky, N., Sein, D., Semmler, T., Shi, X., Stepanek, C., Streffing, J., Wang, Q., Wekerle, C., Yang, H., and Jung, T.: Evaluation of FESOM2.0 Coupled to ECHAM6.3: Preindustrial and High- ResMIP Simulations, 2019. J. Adv. Model. Earth Sy., 11, 3794–3815, https://doi.org/10.1029/2019MS001696

Sime, L. C., K. E. Kohfeld, C. Le Quéré, E. W. Wolff, A. M. de Boer, R. M. Graham, and L. Bopp, 2013: Southern Hemisphere westerly wind changes during the Last Glacial Maximum: Model–data comparison. *Quat. Sci. Rev.*, **64**, 104–120, https://doi.org/10.1016/j.quascirev.2012.12.008.

Sugden, D. E., N. R. J. Hulton, and R. S. Purves (2002), Modelling the inception of the Patagonian icesheet, Quat. Int., 95 – 96, 55 – 64. DOI:10.1016/S0277-3791(01)00103-2

Sutherland, J. L., Carrivick, J. L., Gandy, N., Shulmeister, J., Quincey, D. J., and Cornford, S. L.: Proglacial Lakes Control Glacier Geometry and Behavior During Recession. 2020. Geophys. Res. Lett., 47, e2020GL088865, https://doi.org/10.1029/2020GL088865

Tarasov, L. and Peltier, R. W.: Impact of thermomechanical ice sheet coupling on a model of the 100 kyr ice age cycle. 1999. J. Geophys. Res.-Atmos., 104, 9517–9545

Tozer, B., Sandwell, D.T., Smith, W.H.F., Olsen, S.C., Beale, J.R., Wessel, P. Global Bathymetry and Topography at 15 Arc Sec: SRTM15+. 2019. Earth and Space Science. 6, 10, 1847-1864. https://doi.org/10.1029/2019EA000658

Tigchelaar, M., Timmermann, A., Friedrich, T., Heinemann, M., and Pollard, D.: Nonlinear response of the Antarctic Ice Sheet to late Quaternary Sea level and climate forcing, The Cryosphere, 13, 2615–2631, https://doi.org/10.5194/tc-13-2615-2019, 2019.

Toggweiler, J.R., Russell, J.L., Carson, S.R. Midlatitude westerlies, atmospheric CO_2, and climate change during the ice ages. 2006. Paleoceanography and Paleoclimatology. 21, https://doi.org/10.1029/2005PA001154

Troch, M., Bertrand, S., Lange, C.B., Cardenas, P., Arz, H., Pantoja-Gutierrez, S., De Pol-Holz R., Kilian, R. Glacial isostatic adjustment near the center of the former Patagonian Ice Sheet (48S) during the last 16.5 kyr. Quaternary Science Reviews. 277. https://doi.org/10.1016/j.quascirev.2021.107346

Yan, Q., Wei, T., Zhang, Z. Modeling the climate sensitivity of Patagonian glaciers and their responses to climatic change during the global last glacial maximum. 2022. Quat. Sci. Rev., 288. https://doi.org/10.1016/j.quascirev.2022.107582

Zech, J., Terrizzano, C.M., García Morabito, E., Veit, H., Zech, R., 2017. Timing and extent of late Pleistocene glaciation in the arid Central Andes of Argentina and Chile (22°-41°S). Geogr. Res. Lett. 43, 697–718. https://doi.org/10.18172/cig.3235.